Numer. Math. (2006) 103: 435–459
DOI 10.1007/s00211-006-0683-0

Numerische Mathematik

R. Hiptmair · G. Widmer · J. Zou

Auxiliary space preconditioning in $H_0(\mathbf{curl};\Omega)$

Received: 2 March 2005 / Revised: 21 December 2005 / Published Online: 31 March 2006

Abstract We adapt the principle of auxiliary space preconditioning as presented in [J. Xu, *The auxiliary space method and optimal multigrid preconditioning techniques for unstructured grids*, Computing, 56 (1996), pp. 215–235.] to $\boldsymbol{H}(\mathbf{curl};\omega)$-elliptic variational problems discretized by means of edge elements. The focus is on theoretical analysis within the abstract framework of subspace correction. Employing a Helmholtz-type splitting of edge element vector fields we can establish asymptotic h-uniform optimality of the preconditioner defined by our auxiliary space method.

Mathematics Subject Classifications 65N22 · 65F10 · 65N30 · 65N55

1 Introduction

Given a bounded Lipschitz domain $\Omega \subset \mathbb{R}^3$, we are concerned with solving the boundary value problem

This author was fully supported by Hong Kong RGC grant (Project No. 403403).

This author acknowledges the support from a Direct Grant of CUHK during his visit at The Chinese University of Hong Kong.

R. Hiptmair(✉)
SAM, ETZ Zürich, 8092 Zürich,
E-mail: hiptmair@sam.math.ethz.ch

G. Widmer
SAM, ETH Zürich, 8092 Zürich,
E-mail: gisela.widmer@sam.math.ethz.ch

J. Zou
Department of Mathematics, The Chinese University of Hong Kong, Shatin, N.T., Hong Kong
E-mail: zou@math.cuhk.edu.hk

$$\mathbf{curl}\,\mathbf{curl}\,\mathbf{u} + \mathbf{u} = \mathbf{f} \quad \text{in } \Omega, \quad \mathbf{u_t} = 0 \quad \text{on } \partial\Omega, \tag{1.1}$$

where $\mathbf{f} \in (L^2(\Omega))^3$ and $\mathbf{u_t}$ stands for the tangential trace of the vector field $\mathbf{u}$. Of course, (1.1) could be supplemented by coefficients with spatial variation and these will usually occur when (1.1) is used to model, e.g., low frequency electromagnetic fields [4]. However, in order to keep the presentation focused, we forgo the treatment of variable coefficients. This generalization will be discussed in a few remarks.

The weak formulation of (1.1) is straightforward and reads: seek $\mathbf{u} \in \boldsymbol{H_0}(\mathbf{Curl}; \boldsymbol{\Omega})$ such that

$$a(\mathbf{u}, \mathbf{v}) := \int_\Omega \mathbf{curl}\,\mathbf{u} \cdot \mathbf{curl}\,\mathbf{v} + \mathbf{u} \cdot \mathbf{v}\,\mathrm{d}\mathbf{x} = \int_\Omega \mathbf{f} \cdot \mathbf{v}\,\mathrm{d}\mathbf{x} \quad \forall \mathbf{v} \in \boldsymbol{H}_0(\mathbf{curl}; \Omega)\ . \tag{1.2}$$

For the definition and properties of the function spaces used in this paper we refer to [7, Ch. 1]. In fact, $a(\cdot, \cdot)$ agrees with the natural inner product of the Hilbert space $\boldsymbol{H}_0(\mathbf{curl}; \Omega)$. This ensures existence and uniqueness of solutions of (1.2).

The large sparse symmetric positive definite linear system of equations arising from a finite element Galerkin discretization of (1.2) calls for efficient preconditioning. The search for preconditioners can be guided by the insight that (1.1) is close kin to

$$-\Delta u + u = f \quad \text{in } \Omega \quad , \quad u = 0 \quad \text{on } \Omega. \tag{1.3}$$

In fact, both boundary value problems arise from a single formula when stated in the calculus of differential forms [13]. This suggests that established concepts for preconditioning in the case of second order elliptic boundary value problems carry over to (1.1), with some adjustments, though, in order to deal with the kernel of the **curl**-operator. This guideline has proved very successful in the case of multigrid methods [1, 9, 12] and various domain decomposition approaches [8, 16–18, 27].

Now we set out to perform the adaptation for another powerful idea developed for (1.3): the idea of *auxiliary space preconditioning* [5, 6, 29]. Taking the cue from [12], we supplement the raw principle of auxiliary space preconditioning with a special treatment of **curl**-free functions. This gives rise to the algorithm discussed in Section 4. A key tool in its theoretical analysis will be a regular *Helmholtz-type decomposition* of $\boldsymbol{H}_0(\mathbf{curl}; \Omega)$ [14, 15, 21]. Details will be given in Section 5. The final result is that the new auxiliary space method for (1.1) actually provides an asymptotically optimal preconditioner, whose performance does not degrade as the resolution of the mesh is increased.

The relevance of auxiliary space preconditioning is due to the fact that it targets linear systems of equations that emerge from finite element discretization on a big unstructured mesh for which no refinement hierarchy is available. This is exactly the class of problems for which algebraic multigrid (AMG) has been conceived [23, 26]. Very efficient AMG algorithms are available for (1.3), but AMG approaches to (1.1) fail to deliver the usual mesh-independent multigrid efficiency [2, 22]. This can only be achieved by geometric multigrid algorithms that rely on nested meshes [1, 12, 25].

The auxiliary space method manages to harness the power of standard multigrid by employing auxiliary meshes that, unlike the original unstructured mesh,

allow simple geometric coarsening [29]. Hence, in combination with geometric multigrid, it achieves asymptotically optimal multigrid efficiency. In this respect, the auxiliary space method is clearly superior to all other preconditioners available for (1.1) when discretized on large generically unstructured meshes.

2 Auxiliary space theory

Auxiliary space methods extend the idea of subspace correction schemes for symmetric positive definite (s.p.d.) variational problems [28]. A general abstract theory has been developed in [5, 10, 29]. Here, we briefly review a specialized version, tailored to what is needed for the analysis of our concrete algorithm.

Write V_h for the finite element trial space used to discretize a variational problem with s.p.d. bilinear form $a : V_h \times V_h \mapsto \mathbb{R}$, which induces the energy norm $\|\cdot\|_A := a(\cdot,\cdot)^{\frac{1}{2}}$. The essential ingredients for an auxiliary space preconditioner is the auxiliary space V_a also equipped with a s.p.d. bilinear form $b(\cdot,\cdot)$ (inducing norm $\|\cdot\|_B := b(\cdot\,\cdot)^{\frac{1}{2}}$) and a linear prolongation operator $I_h : V_a \mapsto V_h$. In addition, following [5], the algorithm involves a local smoothing operation based on a decomposition of V_h into subspaces

$$V_h = V_1 + \cdots + V_N\ , \quad N \in \mathbb{N}. \tag{2.1}$$

When splitting a function according to (2.1), the combined energies of the parts must bound the energy of the function, that is, we assume

$$\exists c_0 > 0 : \quad \|v_h\|_A^2 \le c_0 \sum_{i=1}^{N} \|v_i\|_A^2 \quad \forall v_h = \sum_{i=1}^{N} v_i \in V_h,\ v_i \in V_i. \tag{2.2}$$

Let us write V_h' for the dual space of V_h, V_i' for the dual space of V_i ($1 \le i \le N$), and let $A_h : V_h \mapsto V_h'$ be the operator associated with $a(\cdot,\cdot)$. Then the corresponding additive preconditioner $M_h : V_h' \mapsto V_h$ for operator A_h is defined by

$$M_h := \sum_{i=1}^{N} I_i A_i^{-1} I_i' + I_h B_a^{-1} I_h'\ , \tag{2.3}$$

where $A_i : V_i \mapsto V_i'$ and $B_a : V_a \mapsto V_a'$ denote, respectively, the local operator associated with $a(\cdot,\cdot)$ on V_i and the operator induced by $b(\cdot,\cdot)$ on V_a, while $I_i : V_i \mapsto V_h$ represents the natural embedding, $I_i' : V_h' \mapsto V_i'$ and $I_h' : V_h' \mapsto V_a'$ are, respectively, the adjoint operators of I_i and I_h.

Two constants are crucial in the abstract convergence theory presented in [5]. The first measures the stability of the splitting (2.1) plus the auxiliary space

$$K_0 := \sup_{v_h \in V_h \setminus \{0\}} \frac{\inf\left\{\sum_{i=1}^{N} \|v_i\|_A^2 + \|v_a\|_B^2\ ,\ v_i \in V_i, v_a \in V_a,\ \sum_{i=1}^{N} v_i + I_h v_a = v_h\right\}}{\|v_h\|_A^2}. \tag{2.4}$$

The second agrees with the operator norm of the prolongation

$$\omega_0 := \max\left\{1, \sup_{v_a \in V_a \setminus \{0\}} \frac{\|I_h v_a\|_A}{\|v_a\|_B}\right\} . \tag{2.5}$$

Lemma 2.1 *The spectral condition number of $M_h A_h$ from* (2.3) *is bounded by*

$$\kappa(M_h A_h) \leq (c_0 + \omega_0^2) K_0 .$$

Proof To begin with, we note a useful identity: for all $v_h \in V_h$

$$b(B_a^{-1} I_h' A_h v_h, B_a^{-1} I_h' A_h v_h) = \left\langle I_h' A_h v_h, B_a^{-1} I_h' A_h v_h \right\rangle = a(v_h, I_h B_a^{-1} I_h' A_h v_h) . \tag{2.6}$$

Next, we pick any $v_h \in V_h$ and write $v_h = I_h v_a + \sum_{i=1}^N v_i$ for a decomposition in (2.4) that realizes the infimum. Applying the Cauchy-Schwarz inequality twice, we obtain the estimate $\geq K_0^{-1}$ for the smallest eigenvalue of $M_h A_h$:

$$\begin{aligned} a(v_h, v_h) &= a(v_h, I_h v_a + \sum_{i=1}^N v_i) = b(B_a^{-1} I_h' A_h v_h, v_a) + \sum_{i=1}^N a(P_i v_h, v_i) \\ &\leq \|v_a\|_B \left\| B_a^{-1} I_h' A_h v_h \right\|_B + \sum_{i=1}^N \|P_i v_h\|_A \|v_i\|_A \\ &\overset{(2.6)}{\leq} \left(\|v_a\|_B^2 + \sum_{i=1}^N \|v_i\|_A^2 \right)^{\frac{1}{2}} a(M_h A_h v_h, v_h)^{\frac{1}{2}} . \end{aligned}$$

Here, $P_i : V_h \mapsto V_i$ denotes the $a(\cdot,\cdot)$-orthogonal projection. Further, we can separately estimate the summands in

$$a(M_h A_h v_h, v_h) = a(I_h B_a^{-1} I_h' A_h v_h, v_h) + a\left(\sum_{i=1}^N P_i v_h, v_h \right),$$

For the first, we use (2.6) and get

$$\begin{aligned} a(I_h B_a^{-1} I_h' A_h v_h, v_h) &= \left\| B_a^{-1} I_h' A_h v_h \right\|_B^2 = \sup_{w_a \in V_a \setminus \{0\}} \frac{b(B_a^{-1} I_h' A_h v_h, w_a)^2}{\|w_a\|_B^2} \\ &= \sup_{w_a \in V_a \setminus \{0\}} \frac{\langle A_h v_h, I_h w_a \rangle^2}{\|w_a\|_B^2} \\ &\leq \sup_{w_a \in V_a \setminus \{0\}} \frac{\|v_h\|_A^2 \, \|I_h w_a\|_A^2}{\|w_a\|_B^2} \leq \omega_0^2 \|v_h\|_A^2 . \end{aligned}$$

The second can be tackled by the Cauchy-Schwarz inequality, inequality (2.2), and exploiting the properties of the $a(\cdot,\cdot)$-orthogonal projectors P_i:

$$\begin{aligned} a\left(\sum_{i=1}^{N} P_i v_h, v_h\right) &\leq a\left(\sum_{i=1}^{N} P_i v_h, \sum_{i=1}^{N} P_i v_h\right)^{\frac{1}{2}} \|v_h\|_A \\ &\leq c_0 \left(\sum_{i=1}^{N} a(P_i v_h, P_i v_h)\right)^{\frac{1}{2}} \|v_h\|_A \\ &= c_0 a\left(\sum_{i=1}^{N} P_i v_h, v_h\right)^{\frac{1}{2}} \cdot \|v_h\|_A \,. \end{aligned}$$

This yields the bound $(c_0 + \omega_0^2)$ for the largest eigenvalue of $M_h A_h$. □

In practice, a "semi-multiplicative" variant of the auxiliary space method is usually more efficient. It gives rise to the following modified preconditioner

$$M_h^m A_h := \left(Id - \prod_{i=N}^{1} (Id - P_i) \cdot \prod_{i=1}^{N} (Id - P_i) \right) + \omega I_h B_a^{-1} I_h' A_h, \tag{2.7}$$

where $\omega > 0$ is a damping parameter, which may be set to 1. From [30, Sect. 4] we learn that an analogue of Lemma 2.1 will still hold for $M_h^m A_h$.

3 Edge elements

Let Ω be polyhedral and equipped with an oriented unstructured regular tetrahedral mesh $\mathcal{T}_h$ in the sense of [14, Def. 3]. We gauge the quality of $\mathcal{T}_h$ by means of its shape regularity measure [5, Sect. 3]

$$\rho(\mathcal{T}_h) := \max_{K\in\mathcal{T}_h} \frac{h_K}{r_K}, \quad \begin{aligned} h_K &:= \max\{|\mathbf{x}-\mathbf{y}| : \mathbf{x},\mathbf{y} \in K\}, \\ r_K &:= \max\{r > 0 : \exists \mathbf{x} \in K;\ |\mathbf{x}-\mathbf{y}| < r \ \Rightarrow\ \mathbf{y} \in K\}. \end{aligned} \tag{3.1}$$

The locally constant meshwidth function $h \in L^\infty(\Omega)$ of $\mathcal{T}_h$ is defined by

$$h(\mathbf{x}) := h_K \ , \ \text{if } \mathbf{x} \in K. \tag{3.2}$$

Note that, if $\rho(\mathcal{T}_h)$ is small, then the mesh has to be locally uniform in the sense that two adjacent elements $K, K' \in \mathcal{T}_h$ have about the same size[1] $h_K \eqsim h_{K'}$. Moreover, a bound for $\rho(\mathcal{T}_h)$ also imposes a limit on the number of tetrahedra sharing a vertex.

[1] Here and in the sequel, we use the symbols $\lesssim$, $\gtrsim$, and $\eqsim$ to indicate one-sided and two-sided estimates, respectively, whose constants may only depend on Ω and the shape regularity of the finite element meshes involved.

A suitable trial space $\mathbf{E}_h \subset \boldsymbol{H}_0(\mathbf{curl};\Omega)$ for the Galerkin discretization of (1.2) is supplied by lowest order edge elements of the first family [14, 19], that is,

$$\mathbf{E}_h := \{\mathbf{v}_h \in \boldsymbol{H}_0(\mathbf{curl};\Omega) : \mathbf{v}_h|_K(\mathbf{x}) = \mathbf{a}_K + \mathbf{b}_K \times \mathbf{x},\ \mathbf{a}_K, \mathbf{b}_K \in \mathbb{R}^3,\ \forall K \in \mathcal{T}_h\}.$$

Writing $\mathcal{E}_h$ for the set of interior edges of $\mathcal{T}_h$, the global degrees of freedom for $\mathbf{E}_h$ are given by the path integrals

$$\mathbf{v}_h \mapsto \int_e \mathbf{v}_h \cdot \mathrm{d}\vec{s}\ , \quad e \in \mathcal{E}_h. \tag{3.3}$$

They induce the finite element interpolation operator $\mathbf{I}_h : \boldsymbol{C}^0(\bar{\Omega}) \mapsto \mathbf{E}_h$, which can be extended to a continuous operator $\mathbf{I}_h : (\boldsymbol{H}^1(\Omega) \cap \{\mathbf{v} : \mathbf{curl}\,\mathbf{v} \in \boldsymbol{L}^\infty(\Omega)\}) \mapsto \mathbf{E}_h$ [14, Sect. 3.6]. Moreover, we remind that edge elements are an affine equivalent family of finite elements with respect to the pullback transformation, see [14, Sect. 2.2],

$$\widehat{\mathbf{v}}(\widehat{\mathbf{x}}) := \mathsf{B}^T \mathbf{v}(\mathbf{x})\ , \quad \mathbf{x} = \mathsf{B}\widehat{\mathbf{x}} + \mathbf{t}\,, \quad \mathsf{B} \in \mathbb{R}^{3,3},\ \mathbf{t} \in \mathbb{R}^3. \tag{3.4}$$

Affine equivalence techniques can be used to establish the L^2-stability of the finite element basis $\{\mathbf{b}_e\}_{e\in\mathcal{E}_h}$ of $\mathbf{E}_h$ [14, Sect. 3.6]

$$\left\| \sum\nolimits_{e\in\mathcal{E}_h} \alpha_e \mathbf{b}_e \right\|^2_{L^2(\Omega)} \eqsim \sum\nolimits_{e\in\mathcal{E}_h} \alpha_e^2 \left\|\mathbf{b}_e\right\|^2_{L^2(\Omega)} \quad \forall \alpha_e \in \mathbb{R}. \tag{3.5}$$

The standard finite element space $S_h \subset H^1_0(\Omega)$ of piecewise linear finite element functions on $\mathcal{T}_h$ plays an important role as the space of discrete scalar potentials for $\mathbf{E}_h$:

$$\mathbf{grad} S_h \subset \{\mathbf{v}_h \in \mathbf{E}_h : \mathbf{curl}\,\mathbf{v}_h = 0\}\ . \tag{3.6}$$

We adopt the notation $\mathcal{V}_h$ for the set of interior vertices of $\mathcal{T}_h$ and $\{\psi_\mathbf{p}\}_{\mathbf{p}\in\mathcal{V}_h}$ for the standard nodal basis of S_h. It enjoys L^2-stability similar to (3.5). It will be important that $\mathbf{I}_h$ and the standard nodal interpolation operator $\Pi_h : C^0(\bar{\Omega}) \mapsto S_h$ are linked by the *commuting diagram property* [14, Sect. 3.2]

$$\mathbf{I}_h \circ \mathbf{grad} = \mathbf{grad} \circ \Pi_h \quad \text{on } C^1(\bar{\Omega}). \tag{3.7}$$

Of course, (3.7) can be extended to the maximal domains of definition of the involved interpolation operators. There is another relevant commuting diagram property and it involves the space $\mathbf{F}_h$ of $\boldsymbol{H}_0(\mathrm{div};\Omega)$-conforming lowest order face elements, see [14, Sect. 3.2]:

$$\mathbf{F}_h := \{\mathbf{v}_h \in \boldsymbol{H}_0(\mathrm{div};\Omega) : \mathbf{v}_h|_K(\mathbf{x}) = \mathbf{a} + \beta\mathbf{x},\ \mathbf{a} \in \mathbb{R}^3, \beta \in \mathbb{R},\ \forall K \in \mathcal{T}_h\}. \tag{3.8}$$

Its global degrees of freedom boil down to evaluating fluxes through the interior faces of $\mathcal{T}_h$. They give rise to an interpolation operator $\mathbf{J}_h : \boldsymbol{C}^0(\bar{\Omega}) \mapsto \mathbf{F}_h$ that satisfies

$$\mathbf{J}_h \circ \mathbf{curl} = \mathbf{curl} \circ \mathbf{I}_h \quad \text{on } \boldsymbol{C}^1(\bar{\Omega}). \tag{3.9}$$

The implementation of the auxiliary space method relies on the so-called second family of edge elements [20]. The corresponding $\boldsymbol{H}_0(\mathbf{curl};\Omega)$-conforming finite element space on $\mathcal{T}_h$ reads

$$\widetilde{\mathbf{E}}_h := \{\mathbf{v}_h \in \boldsymbol{H}_0(\mathbf{curl};\Omega) : \ \mathbf{v}_{h|K} \in (\mathcal{P}_1(K))^3 \ \forall K \in \mathcal{T}_h\}, \tag{3.10}$$

where $\mathcal{P}_1(K)$ is the space of affine linear functions on K. There are two global degrees of freedom associated with each edge in $\mathcal{E}_h$: beside (3.3) they comprise the first moments

$$\mathbf{v}_h \mapsto \int_e (1-2t)\mathbf{v}_h(t)\cdot \mathrm{d}\vec{s}(t)\ , \quad e \in \mathcal{E}_h,$$

with $0 \le t \le 1$ designating a normalized edge coordinate. Let $\widetilde{\mathbf{I}}_h : \boldsymbol{C}^0(\bar{\Omega}) \mapsto \widetilde{\mathbf{E}}_h$ denote the induced finite element interpolation operator.

On a tetrahedron K with barycentric coordinates $\lambda_1,\ldots,\lambda_4$ the local shape functions of $\widetilde{\mathbf{E}}_h$ are given by

$$\lambda_i \mathbf{grad}\lambda_j - \lambda_j \mathbf{grad}\lambda_i \quad , \quad \mathbf{grad}(3\lambda_i\lambda_j)\,, \quad 1 \le i < j \le 4. \tag{3.11}$$

They can be assembled into a basis $\{\widetilde{\mathbf{b}}_i,\ i = 1,\ldots,2\sharp\mathcal{E}_h\}$ of $\widetilde{\mathbf{E}}_h$. The second group of basis functions from (3.11) agree with the gradients of "quadratic edge bubble functions". This points to a close relationship of $\widetilde{\mathbf{E}}_h$ with the space $\widetilde{S}_h \subset H_0^1(\Omega)$ of piecewise quadratic continuous finite element functions on $\mathcal{T}_h$. In fact, there is a direct sum decomposition corresponding to (3.11)

$$\widetilde{\mathbf{E}}_h = \mathbf{E}_h \oplus \mathbf{grad}(Id - \Pi_h)\widetilde{S}_h. \tag{3.12}$$

Local scaling arguments immediately confirm that this decomposition is $\boldsymbol{L}^2(\Omega)$-stable: For any $\mathcal{T}_h$-piecewise constant positive weighting function $w \in L^\infty(\Omega)$

$$\|w\widetilde{\mathbf{v}}_h\|^2_{L^2(\Omega)} \eqsim \|w\mathbf{v}_h\|^2_{L^2(\Omega)} + \|w\mathbf{grad}\widetilde{\phi}_h\|^2_{L^2(\Omega)}, \tag{3.13}$$

for all $\widetilde{\mathbf{v}}_h = \mathbf{v}_h + \mathbf{grad}\widetilde{\phi}_h \in \widetilde{\mathbf{E}}_h$, $\mathbf{v}_h \in \mathbf{E}_h$, $\widetilde{\phi}_h \in (Id - \Pi_h)\widetilde{S}_h$.

Besides, there is another connection between $\widetilde{S}_h$ and $\widetilde{\mathbf{E}}_h$, which can be expressed by the commuting diagram property

$$\widetilde{\mathbf{I}}_h \circ \mathbf{grad} = \mathbf{grad} \circ \widetilde{\Pi}_h \quad \text{on } C^1(\bar{\Omega})\ , \tag{3.14}$$

where $\widetilde{\Pi}_h$ is nodal interpolation onto $\widetilde{S}_h$.

4 Algorithm

Beside $\mathcal{T}_h$, we introduce an oriented *semi-structured* regular tetrahedral *auxiliary mesh* $\mathcal{T}_a$ such that

$$\bar{\Omega}_a := \bigcup\{\bar{K}_a : \ K_a \in \mathcal{T}_a\} \subset \bar{\Omega}. \tag{4.1}$$

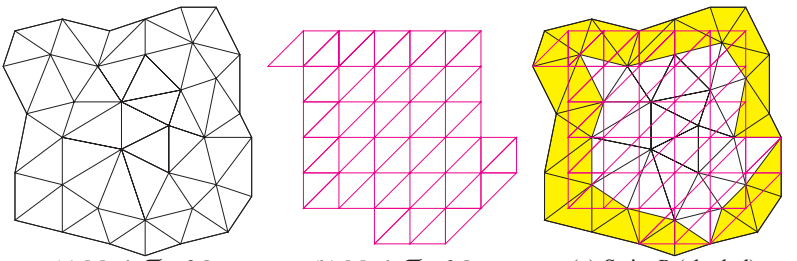

(a) Mesh $\mathcal{T}_h$ of Ω (b) Mesh $\mathcal{T}_a$ of Ω_a (c) Strip B (shaded)

Fig. 4.1 Different quasi-uniform meshes used to specify auxiliary space method

Writing h_a for its meshwidth function, see (3.2), we demand matching local meshwidths in the sense that there is a small constant $C_a > 0$ such that

$$C_a^{-1} h \leq h_a \leq C_a h \quad \text{a.e. in } \Omega_a \ . \tag{4.2}$$

Moreover, we expect $\mathcal{T}_a$ to cover Ω except for a "thin" strip along $\partial\Omega$. Let $\mathcal{V}_\partial$ stand for the vertices of $\mathcal{T}_h$ located on $\partial\Omega$. For $\mathbf{p} \in \mathcal{V}_\partial$ we introduce

$$h_{\mathbf{p}} := \frac{1}{\sharp \mathcal{T}_{\mathbf{p}}} \sum_{K \in \mathcal{T}_{\mathbf{p}}} h_K \quad , \quad \mathcal{T}_{\mathbf{p}} := \{K \in \mathcal{T}_h : \mathbf{p} \in \bar{K}\} \ , \tag{4.3}$$

in order to refer to the average size of tetrahedra adjacent to $\mathbf{p}$. Hence, $h_{\mathbf{p}}$ can be read as local meshwidth at $\mathbf{p}$. The boundary strip (see Fig. 4.1(c) for a 2D illustration)

$$\bar{B} := \bigcup \{\bar{K} \in \mathcal{T}_h : \ K \not\subset \Omega_a\} \tag{4.4}$$

has to be slim, expressed by the requirement that there must exist a small constant $C_\partial > 0$ such that

$$B \subset \bigcup_{\mathbf{p} \in \mathcal{V}_\partial} B_{\mathbf{p}} \quad , \quad B_{\mathbf{p}} := \{\mathbf{x} \in B : \ |\mathbf{x} - \mathbf{p}| < C_\partial h_{\mathbf{p}}\}. \tag{4.5}$$

For the remainder of this paper we will admit that the constants hidden in the symbols $\lesssim$, $\gtrsim$, and $\eqsim$ may also depend on C_a and C_∂.

Apart from (4.2) and (4.5), no further requirements are imposed on $\mathcal{T}_a$. In particular, the cells of $\mathcal{T}_h$ and $\mathcal{T}_a$ can have arbitrary relative positions. Fig. 4.1 depicts a typical two-dimensional situation, where the meshes are rather structured and the auxiliary space is based on a mesh that allows geometric coarsening, *cf.* [29]. Fig. 4.2 illustrates a particular choice of $\mathcal{T}_a$ in the case of local refinement: both meshes undergo refinement in the same part of Ω.

The auxiliary space V_a from Sect. 2 will be chosen as the finite element subspace[2] $\widetilde{\mathbf{E}}_a$ of $\boldsymbol{H}_0(\mathbf{curl}; \Omega_a)$ *generated by the second family of edge elements* (3.10) on $\mathcal{T}_a$. Why not the first family of edge elements as used in $\mathbf{E}_h$ on $\mathcal{T}_h$? The reason

[2] We will consistently tag entities associated with $\mathcal{T}_a$ by a subscript a, whereas relationship with $\mathcal{T}_h$ is expressed by a subscript h.

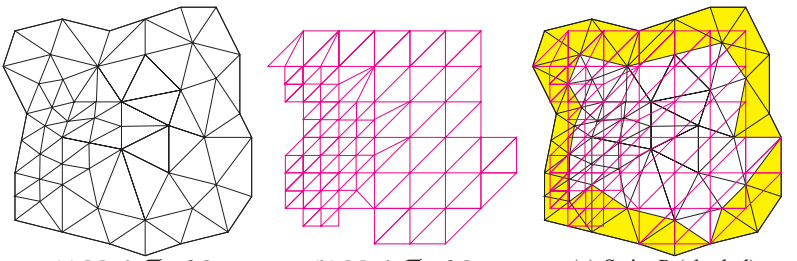

(a) Mesh $\mathcal{T}_h$ of Ω (b) Mesh $\mathcal{T}_a$ of Ω_a (c) Strip B (shaded)

Fig. 4.2 Auxiliary mesh and boundary strip B for locally refined meshes

is that the theoretical analysis of Sect. 5.2 hinges on the fact that only edge element spaces of the second family are rich enough to contain all piecewise linear continuous vector fields. However, the need for second family of edge elements in V_a is not borne out by numerical experiments, see Sect. 6: it is due to limitations of the current theory.

As prolongation operator I_h we choose the finite element interpolation $\mathbf{I}_h : \widetilde{\mathbf{E}}_a \mapsto \mathbf{E}_h$. The splitting (2.1) is inspired by the idea of hybrid smoothing in the context of multigrid for $\boldsymbol{H}(\mathbf{curl};\Omega)$-elliptic variational problems [12, Formula (3.5)]:

$$\mathbf{E}_h = \sum_{e\in\mathcal{E}_h} \mathrm{Span}\,\{\mathbf{b}_e\} + \sum_{\mathbf{p}\in\mathcal{V}_h} \mathrm{Span}\,\{\mathbf{grad}\psi_{\mathbf{p}}\}\,. \tag{4.6}$$

This splitting captures oscillatory **curl**-free error components, *cf.* the discussion in [12, Sect. 3]. Eventually, we simply pick the restriction of $a(\cdot,\cdot)$ from (1.2) to $\widetilde{\mathbf{E}}_a$ as bilinear form $b(\cdot,\cdot)$ on V_a. This tacitly assumes a zero extension to Ω of functions in $\widetilde{\mathbf{E}}_a$. Table 4.1 summarizes how to fit this particular algorithm into the abstract theory of Sect. 2.

In order to give an algebraic description of the resulting auxiliary space preconditioner we have to introduce a few matrices ($\mathcal{E}_a$ are the interior edges of $\mathcal{T}_a$)

$$\begin{aligned}
\mathsf{A} &:= (a(\mathbf{b}_e,\mathbf{b}_{e'}))_{e,e'\in\mathcal{E}_h} && \in \mathbb{R}^{\sharp\mathcal{E}_h,\sharp\mathcal{E}_h}\,,\\
\mathsf{B} &:= (a(\widetilde{\mathbf{b}}_i,\widetilde{\mathbf{b}}_j))_{i,j} && \in \mathbb{R}^{2\sharp\mathcal{E}_a,2\sharp\mathcal{E}_a}\,,\\
\mathsf{L} &:= (l_{e,\mathbf{p}})_{e\in\mathcal{E}_h,\mathbf{p}\in\mathcal{V}_h} && \in \mathbb{R}^{\sharp\mathcal{E}_h,\sharp\mathcal{V}_h} : \mathbf{grad}\psi_{\mathbf{p}} = \textstyle\sum_{e\in\mathcal{E}_h} l_{e,\mathbf{p}}\,\mathbf{b}_e\,,\\
\mathsf{D} &:= (a(\mathbf{grad}\psi_{\mathbf{p}},\mathbf{grad}\psi_{\mathbf{q}}))_{\mathbf{p},\mathbf{q}\in\mathcal{V}_h} && \in \mathbb{R}^{\sharp\mathcal{V}_h,\sharp\mathcal{V}_h}\,,\\
\mathsf{T} &:= (t_{e,i})_{e\in\mathcal{E}_h,i=1,\ldots,2\sharp\mathcal{E}_a} && \in \mathbb{R}^{\sharp\mathcal{E}_h,2\sharp\mathcal{E}_a} : \mathbf{I}_h\widetilde{\mathbf{b}}_i = \textstyle\sum_{e\in\mathcal{E}_h} t_{e,i}\,\mathbf{b}_e.
\end{aligned} \tag{4.7}$$

Table 4.1 Concrete choices for auxiliary space preconditioner in $\boldsymbol{H}(\mathbf{curl};\Omega)$

Sect. 2	Concrete choice for algorithm
V_h	First family edge element space $\mathbf{E}_h$ on $\mathcal{T}_h$
V_a	Second family edge element space $\widetilde{\mathbf{E}}_a$ on $\mathcal{T}_a$
$a(\cdot,\cdot)$	Bilinear form $a(\cdot,\cdot)$ from (1.2) on Ω
$b(\cdot,\cdot)$	Same as $a(\cdot,\cdot)$ but on Ω_a
I_h	Edge element interpolation operator $\mathbf{I}_h$
V_i	(Lumped) Span $\{\mathbf{b}_e\}$ and Span $\{\mathbf{grad}\psi_{\mathbf{p}}\}$

All these matrices have a small number of non-zero entries per row so that matrix-vector products require $O(\sharp\mathcal{E}_h)$ operations in each case. If the costs of solving the linear system with matrix B are ignored, the computational effort for a single evaluation of the preconditioner scales linearly with the size of the stiffness matrix A. A pseudo-code description of an implementation of the preconditioner (2.7) is given in Fig. 4.3.

Remark The construction of a structured auxiliary mesh as those shown in Figs. 4.1 and 4.2 can efficiently done by means of octree techniques. In addition, this hierarchical data structure makes it easy to locate cells of the auxiliary mesh.

Remark Any s.p.d. bilinear form $b(\cdot,\cdot)$ that is spectrally equivalent to $a(\cdot,\cdot)$ on V_a can be used to get the correction from the auxiliary space without affecting the asymptotic properties of the method. For instance, the exact solve of $\mathsf{B}\vec{\mathbf{c}}_a = \vec{\mathbf{f}}_a$ (see Fig. 4.3) can be replaced by a V-cycle of geometric multigrid in $\boldsymbol{H}_0(\mathbf{curl};\Omega)$. This will result in true $O(\sharp\mathcal{E}_h)$ computational costs of a single evaluation.

Remark In practice, see Sect. 6, the best performing preconditioner seems to arise from a fully multiplicative implementation of the auxiliary space method, whose implementation is outlined in Fig. 4.4.

5 Convergence analysis

In this section we aim to prove the main theoretical result of this paper. It will first be stated and then we will establish the prerequisites for applying the abstract theory of Sect. 2.

Theorem 5.1 *Under the assumptions made in the previous section the spectral condition number $\kappa(M_h A_h)$ for the auxiliary space method outlined in the previous section only depends on Ω and the shape-regularity measures $\rho(\mathcal{T}_h)$ and $\rho(\mathcal{T}_a)$.*

function $\vec{\mathbf{u}} = M_h^m(\vec{\mathbf{f}})$
{
$\vec{\mathbf{u}} = 0$
Forward Gauss-Seidel sweep(s) on $\mathsf{A}\vec{\mathbf{u}} = \vec{\mathbf{f}}$
Compute residual $\vec{\mathbf{r}} := \vec{\mathbf{f}} - \mathsf{A}\vec{\mathbf{u}}$
Lift residual $\vec{\rho} := \mathsf{L}^T\vec{\mathbf{r}}$
$\vec{\gamma} := 0$; Symmetric Gauss-Seidel on $\mathsf{D}\vec{\gamma} = \vec{\rho}$
Update $\vec{\mathbf{u}} \leftarrow \vec{\mathbf{u}} + \mathsf{L}\vec{\gamma}$
Backward Gauss-Seidel sweep(s) on $\mathsf{A}\vec{\mathbf{u}} = \vec{\mathbf{f}}$
} (Hybrid) Smoothing

Restrict $\vec{\mathbf{f}}_a := \mathsf{T}^T\vec{\mathbf{f}}$
Solve $\mathsf{B}\vec{\mathbf{c}}_a = \vec{\mathbf{f}}_a$
Prolongate (damped) correction $\vec{\mathbf{u}} \leftarrow \vec{\mathbf{u}} + \omega\mathsf{T}\vec{\mathbf{c}}_a$
} Auxiliary space correction
}

Fig. 4.3 Pseudo-code for the evaluation of the semi-multiplicative auxiliary space preconditioner, $\vec{\mathbf{f}}, \vec{\mathbf{u}} \in \mathbb{R}^{\sharp\mathcal{E}_h}$, matrices from (4.7)

function $\vec{\mathbf{u}} = M_h^m(\vec{\mathbf{f}})$
{
$\vec{\mathbf{u}} = 0$

Forward Gauss-Seidel sweep(s) on $\mathsf{A}\vec{\mathbf{u}} = \vec{\mathbf{f}}$ Compute residual $\vec{\mathbf{r}} := \vec{\mathbf{f}} - \mathsf{A}\vec{\mathbf{u}}$ Lift residual $\vec{\rho} := \mathsf{L}^T\vec{\mathbf{r}}$ $\vec{\gamma} := 0$; Forward Gauss-Seidel on $\mathsf{D}\vec{\gamma} = \vec{\rho}$ Update $\vec{\mathbf{u}} \leftarrow \vec{\mathbf{u}} + \mathsf{L}\vec{\gamma}$	(Hybrid) Pre-smoothing
Compute residual $\vec{\mathbf{r}} := \vec{\mathbf{f}} - \mathsf{A}\vec{\mathbf{u}}$ Restrict $\vec{\mathbf{r}}_a := \mathsf{T}^T\vec{\mathbf{r}}$ Solve $\mathsf{B}\vec{\mathbf{e}}_a = \vec{\mathbf{r}}_a$ Prolongate correction $\vec{\mathbf{u}} \leftarrow \vec{\mathbf{u}} + \mathsf{T}\vec{\mathbf{e}}_a$	Auxiliary space correction
Compute residual $\vec{\mathbf{r}} := \vec{\mathbf{f}} - \mathsf{A}\vec{\mathbf{u}}$ Lift residual $\vec{\rho} := \mathsf{L}^T\vec{\mathbf{r}}$ $\vec{\gamma} := 0$; Backward Gauss-Seidel on $\mathsf{D}\vec{\gamma} = \vec{\rho}$ Update $\vec{\mathbf{u}} \leftarrow \vec{\mathbf{u}} + \mathsf{L}\vec{\gamma}$ Backward Gauss-Seidel sweep(s) on $\mathsf{A}\vec{\mathbf{u}} = \vec{\mathbf{f}}$	(Hybrid) Post-smoothing

Fig. 4.4 Pseudo-code for the evaluation of the multiplicative auxiliary space preconditioner, $\vec{\mathbf{f}}, \vec{\mathbf{u}} \in \mathbb{R}^{\sharp\mathcal{E}_h}$, matrices from (4.7)

To begin with, (2.2) is a fairly straightforward estimate for decompositions (2.1) based on locally supported basis functions. For any $\mathbf{v}_h \in \mathbf{E}_h$, $\mathbf{v}_h = \sum_{e\in\mathcal{E}_h} a_e\mathbf{b}_e$, $\alpha_e \in \mathbb{R}$,

$$\|\mathbf{v}_h\|_A^2 = \left\|\sum\nolimits_{e\in\mathcal{E}_h} a_e\mathbf{b}_e\right\|_A^2 = \sum_{K\in\mathcal{T}_h} \left\|\sum\nolimits_{j=1}^{6} \alpha_{j,K}\mathbf{b}_{j,K}\right\|_{A,K}^2 ,$$

where $\mathbf{b}_{j,K}$, $j = 1,\ldots,6$, are the nontrivial restrictions of edge element basis functions to the element K. The Cauchy-Schwarz inequality yields

$$\begin{aligned}\|\mathbf{v}_h\|_A^2 &\le 6 \sum_{K\in\mathcal{T}_h} \sum\nolimits_{j=1}^{6} |\alpha_{j,K}|^2 \left\|\mathbf{b}_{j,K}\right\|_{A,K}^2 \\ &= 6 \sum_{K\in\mathcal{T}_h} \sum_{e\in\mathcal{E}_h} |\alpha_e|^2 \|\mathbf{b}_e\|_{A,K}^2 = 6 \sum_{e\in\mathcal{E}_h} \|\alpha_e\mathbf{b}_e\|_A^2 .\end{aligned}$$

A similar argument applies to nodal decompositions of S_h, and we conclude (2.2) with $c_0 = 6$.

Next, we investigate the continuity of $\mathbf{I}_h$ in order to establish mesh-independence of ω_0.

Lemma 5.2 *Under the assumptions (4.2) and (4.5) on $\mathcal{T}_h$ and $\mathcal{T}_a$ there holds true*

$$\|\mathbf{I}_h\mathbf{v}_a\|_A \lesssim \|\mathbf{v}_a\|_A \quad \forall\, \mathbf{v}_a \in \widetilde{\mathbf{E}}_a .$$

Proof Consider an arbitrary element $K \in \mathcal{T}_h$. One can show by a simple scaling argument the following equivalence for all $\mathbf{v}_h \in \mathbf{E}_h$ and $\mathbf{v}_a \in \widetilde{\mathbf{E}}_a$

$$\|\mathbf{v}_h\|^2_{L^2(K)} \eqsim h_K \sum_{e\in\mathcal{E}_K} \left(\int_e \mathbf{v}_h \cdot \mathrm{d}\vec{s}\right)^2, \tag{5.1}$$

$$\|\mathbf{v}_a\|^2_{L^2(K_a)} \eqsim h_{K_a} \sum_{e\in\mathcal{E}_{K_a}} \left\{\left(\int_e \mathbf{v}_a \cdot \mathrm{d}\vec{s}\right)^2 + \left(\int_e (1-2t)\mathbf{v}_a(t) \cdot \mathrm{d}\vec{s}(t)\right)^2\right\}. \tag{5.2}$$

If $\mathbf{v}_h = \mathbf{I}_h\mathbf{v}_a$ for some $\mathbf{v}_a \in \widetilde{\mathbf{E}}_a$ (which is supposed to have been extended by zero outside Ω_a), the very definition of $\mathbf{I}_h$ implies

$$\|\mathbf{I}_h\mathbf{v}_a\|^2_{L^2(K)} \lesssim h_K^3 \, \|\mathbf{v}_a\|^2_{L^\infty(U_K)}\,, \tag{5.3}$$

with $U_K := \bigcup\{K_a \in \mathcal{T}_a,\ K_a \cap K \neq \emptyset\}$, see Fig. 5.1. Inspecting the basis functions from (3.11) we find that for a $K_a \in \mathcal{T}_a$

$$\begin{aligned}\|\mathbf{v}_a\|_{L^\infty(K_a)} &\lesssim h_{K_a}^{-1} \sum_{e\in\mathcal{E}_{K_a}} \left(\left|\int_e \mathbf{v}_a \cdot \mathrm{d}\vec{s}\right| + \left|\int_e (1-2t)\mathbf{v}_a(t) \cdot \mathrm{d}\vec{s}(t)\right|\right)\\ &\lesssim h_{K_a}^{-1} \left(\sum_{e\in\mathcal{E}_{K_a}} \left\{\left(\int_e \mathbf{v}_a \cdot \mathrm{d}\vec{s}\right)^2 + \left(\int_e (1-2t)\mathbf{v}_a(t) \cdot \mathrm{d}\vec{s}(t)\right)^2\right\}\right)^{\frac{1}{2}}.\end{aligned}$$

From this and (5.2) we infer

$$\|\mathbf{v}_a\|^2_{L^\infty(K_a)} \lesssim h_{K_a}^{-3} \, \|\mathbf{v}_a\|^2_{L^2(K_a)}\,. \tag{5.4}$$

Combining the estimates, we arrive at

$$\|\mathbf{I}_h\mathbf{v}_a\|^2_{L^2(K)} \lesssim h_K^3 \sum_{K_a\in U_K} h_{K_a}^{-3} \, \|\mathbf{v}_a\|^2_{L^2(K_a)}\,. \tag{5.5}$$

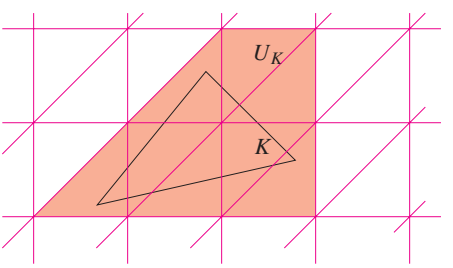

Fig. 5.1 Proof of Lemma 5.2: neighborhood U_K in 2D

Now we appeal to the matching condition (4.2) and the local quasi-uniformity of the meshes, which give us $h_K \eqsim h_{K_a}$ for all $K_a \in U_K$. The finite overlap property of the neighborhoods U_K finally confirms

$$\|\mathbf{I}_h \mathbf{v}_a\|_{L^2(\Omega)} \lesssim \|\mathbf{v}_a\|_{L^2(\Omega_a)} . \tag{5.6}$$

In order to show

$$\|\mathbf{curl}\, \mathbf{I}_h \mathbf{v}_a\|_{L^2(\Omega)} \lesssim \|\mathbf{curl}\, \mathbf{v}_a\|_{L^2(\Omega)} \tag{5.7}$$

we need merely resort to the commuting diagram property (3.9). Then the proof can be carried out as above with face elements and their degrees of freedom replacing edge elements and edge path integrals. We skip the details. □

Summing up, we have shown $\omega_0 \lesssim 1$ in (2.5) for the concrete choices for V_h, V_a, and I_h given in Tab. 4.1. It remains to prove that K_0 from (2.4) does not depend on the sizes of elements of $\mathcal{T}_h$.

5.1 Auxiliary space decomposition in $H_0^1(\Omega)$

To fix ideas and provide estimates for later use, we briefly recall the proof of the stability of the auxiliary space decomposition of S_h. More details can be found in [29, Sect. 4] and [5, Sect. 3].

We pick an arbitrary $\varphi_h \in S_h$. The crucial idea is to separate off a part $\beta_h \in S_h$ close to the boundary:

$$\beta_h(\mathbf{p}) := \begin{cases} \varphi_h(\mathbf{p}) & \text{for } \mathbf{p} \in \mathcal{V}_h \cap \bar{B} , \\ 0 & \text{for } \mathbf{p} \in \mathcal{V}_h \cap (\Omega \setminus \bar{B}) . \end{cases} \tag{5.8}$$

Lemma 5.3 (*cf.* Lemma 4.2 in [29]) *The following estimates hold with constants only depending on $\rho(\mathcal{T}_h)$ and C_∂*

$$\left\| h^{-1} \beta_h \right\|_{L^2(\Omega)} \lesssim |\beta_h|_{H^1(\Omega)} , \quad |\beta_h|_{H^1(\Omega)} \lesssim |\varphi_h|_{H^1(\Omega)} .$$

Proof We invoke the L^2-stability of the nodal basis of S_h and then use local Poincaré-Friedrichs inequalities (since $\beta_h = 0$ on $\partial\Omega$), and the finite overlap property of the neighborhoods $B_{\mathbf{p}}$ defined in (4.5):

$$\begin{aligned} \left\| h^{-1} \beta_h \right\|^2_{L^2(\Omega)} \lesssim \left\| h^{-1} \beta_h \right\|^2_{L^2(B)} &\lesssim \sum_{\mathbf{p} \in \mathcal{V}_\partial} h_{\mathbf{p}}^{-2} \, \|\beta_h\|^2_{L^2(B_{\mathbf{p}})} \\ &\lesssim \sum_{\mathbf{p} \in \mathcal{V}_\partial} h_{\mathbf{p}}^{-2} \operatorname{diam}(B_{\mathbf{p}})^2 \, |\beta_h|^2_{H^1(B_{\mathbf{p}})} \\ &\lesssim \sum_{\mathbf{p} \in \mathcal{V}_\partial} |\beta_h|^2_{H^1(B_{\mathbf{p}})} \lesssim |\beta_h|^2_{H^1(B)} . \end{aligned}$$

Applying local inverse inequalities settles the second estimate

$$|\beta_h|_{H^1(\Omega)} \lesssim \left\| h^{-1} \beta_h \right\|_{L^2(\Omega)} \lesssim \left\| h^{-1} \beta_h \right\|_{L^2(B)} \lesssim |\beta_h|_{H^1(B)} \lesssim |\varphi_h|_{H^1(B)} ,$$

because $\beta_h \equiv \varphi_h$ on B. □

Next, recall the concept of *local* quasi-interpolation operators, for instance the one proposed by Scott and Zhang in [24], see also [31]. It provides a local projection $Q_a : H_0^1(\Omega_a) \mapsto S_a$, S_a the space of piecewise linear $H_0^1(\Omega_a)$-conforming finite element functions on $\mathcal{T}_a$, with the following properties: for all $\varphi_a \in H_0^1(\Omega_a)$

$$\left\| h_a^{-1}(\varphi_a - Q_a\varphi_a) \right\|_{L^2(\Omega_a)} \lesssim |\varphi_a|_{H^1(\Omega_a)}\,, \tag{5.9}$$

$$|Q_a\varphi_a|_{H^1(\Omega_a)} \lesssim |\varphi_a|_{H^1(\Omega_a)}\,. \tag{5.10}$$

Further, one can establish the following estimates for the nodal interpolation operator Π_h, see [6, Lemma 1], [29, Lemma 4.1] and the proof of Lemma 5.5 below:

$$\left\| h^{-1}(Id - \Pi_h)\varphi_a \right\|_{L^2(\Omega)} \lesssim |\varphi_a|_{H^1(\Omega)} \quad \forall\, \varphi_a \in S_a. \tag{5.11}$$

Keeping in mind that $\mu_h := \varphi_h - \beta_h$ is supported in $\bar{\Omega}_0$, $\Omega_0 := \Omega \setminus \bar{B}$, estimates (5.9), (5.10), and (5.11) immediately give

$$\left\| h^{-1}(Id - \Pi_h Q_a)\mu_h \right\|_{L^2(\Omega)} \lesssim |\mu_h|_{H^1(\Omega)}\,. \tag{5.12}$$

Now we are in a position to study the H^1-stability of the splitting (For the sake of clarity it has been related to the abstract decomposition discussed in Sect. 2.)

$$\begin{array}{ccccc} \varphi_h & = & (\beta_h + (Id - \Pi_h Q_a)\mu_h) & + & \Pi_h(Q_a\mu_h). \\ \cap & & \updownarrow & & \updownarrow \\ V_h & = & V_1 + \cdots + V_N & + & I_h\, V_a \end{array} \tag{5.13}$$

By virtue of (5.12), Lemma 5.3, L^2-stability of the nodal basis $\{\psi_{\mathbf{p}}\}_{\mathbf{p}\in\mathcal{V}_h}$, and the fact that $|\psi_{\mathbf{p}}|_{H^1(\Omega)} \lesssim \|h^{-1}\psi_{\mathbf{p}}\|_{L^2(\Omega)}$, $\forall\, \mathbf{p} \in \mathcal{V}_h$, we conclude that the first term in the splitting can be decomposed into contributions of basis functions in a H^1-stable manner:

$$\beta_h + (Id - \Pi_h Q_a)\mu_h = \sum_{\mathbf{p}\in\mathcal{V}_h} \alpha_{\mathbf{p}}\psi_{\mathbf{p}}, \tag{5.14}$$

$$\sum_{\mathbf{p}\in\mathcal{V}_h} \alpha_{\mathbf{p}}^2 |\psi_{\mathbf{p}}|^2_{H^1(\Omega)} \lesssim |\beta_h|^2_{H^1(\Omega)} + |\mu_h|^2_{H^1(\Omega)}. \tag{5.15}$$

Further, Lemma 5.3 also implies $|\mu_h|_{H^1(\Omega)} \lesssim |\varphi_h|_{H^1(\Omega)}$ and along with (5.9) this ensures the H^1-stability of (5.13) with constants only depending on shape regularity, C_∂ and C_a.

5.2 Auxiliary space decomposition in $\boldsymbol{H}_0(\mathbf{curl};\Omega)$

Given $\mathbf{v}_h \in \mathbf{E}_h$ we have to find $\mathbf{q}_h \in \mathbf{E}_h$, $\zeta_h \in S_h$, and $\widetilde{\mathbf{w}}_a \in \widetilde{\mathbf{E}}_a$ such that

$$\mathbf{v}_h = \mathbf{q}_h + \mathbf{grad}\zeta_h + \mathbf{I}_h\widetilde{\mathbf{w}}_a, \tag{5.16}$$

and

$$\left\| h^{-1}\mathbf{q}_h \right\|_{L^2(\Omega)} \lesssim \|\mathbf{v}_h\|_A \;,\; \left\| h^{-1}\zeta_h \right\|_{L^2(\Omega)} \lesssim \|\mathbf{v}_h\|_A \;,\; \|\mathbf{w}_a\|_A \lesssim \|\mathbf{v}_h\|_A\,. \tag{5.17}$$

Thanks to the L^2-stability of the bases of $\mathbf{E}_h$ and S_h and local inverse estimates, *cf.* the arguments at the end of Sect. 5.1, the first two estimates ensure that $\mathbf{q}_h + \mathbf{grad}\zeta_h$ possesses a uniformly stable splitting according to (4.6). Together with the third inequality of (5.17), it is then straightforward that $K_0 \lesssim 1$.

Our key tool is the stable regular Helmholtz-type decomposition from [14, Lemma 2.4], [21, Lemma 2.2]

$$\boldsymbol{H}_0(\mathbf{curl};\Omega) = \boldsymbol{H}_0^1(\Omega) + \mathbf{grad}\, H_0^1(\Omega)\ .$$

This guarantees that we can find $\mathbf{z} \in \boldsymbol{H}_0^1(\Omega)$ and $\phi \in H_0^1(\Omega)$ such that $\mathbf{v}_h = \mathbf{z} + \mathbf{grad}\phi$ and

$$|\mathbf{z}|_{H^1(\Omega)} \lesssim \|\mathbf{curl}\,\mathbf{v}_h\|_{L^2(\Omega)}\,, \quad |\phi|_{H^1(\Omega)} \lesssim \|\mathbf{v}_h\|_A\,. \tag{5.18}$$

The Helmholtz-type regular decomposition of $\mathbf{v}_h$ fails to provide components in finite element space. So the next step is about retrieving a fully discrete splitting.

To that end we introduce a vectorial quasi-interpolation operator $\mathbf{Q}_h : \boldsymbol{H}_0^1(\Omega) \mapsto \mathbf{S}_h := (S_h)^3$ by applying the standard Scott-Zhang operator $Q_h : H_0^1(\Omega) \mapsto S_h$ to the components of vector fields. The operator $\mathbf{Q}_h$ enjoys continuity and stability properties analoguous to (5.9) and (5.10), which means that $\mathbf{z}_h := \mathbf{Q}_h\mathbf{z}$ satisfies

$$|\mathbf{z}_h|_{H^1(\Omega)} \lesssim |\mathbf{z}|_{H^1(\Omega)}\,, \quad \|h^{-1}(\mathbf{z}-\mathbf{z}_h)\|_{L^2(\Omega)} \lesssim |\mathbf{z}|_{H^1(\Omega)}\,. \tag{5.19}$$

This gives us the intermediate splitting

$$\mathbf{v}_h = \mathbf{z}_h + (\mathbf{z}-\mathbf{z}_h) + \mathbf{grad}\phi. \tag{5.20}$$

In order to return to the discrete setting completely, we apply edge element interpolation $\widetilde{\mathbf{I}}_h$ onto the second family edge element space $\widetilde{\mathbf{E}}_h$: by the commuting diagram property (3.14) we obtain

$$\mathbf{v}_h = \mathbf{z}_h + \widetilde{\mathbf{I}}_h(\mathbf{z}-\mathbf{z}_h) + \mathbf{grad}\widetilde{\Pi}_h\phi. \tag{5.21}$$

Here, the second family of edge elements comes very handy, because $\mathbf{S}_h \subset \widetilde{\mathbf{E}}_h$ so that $\widetilde{\mathbf{I}}_h\mathbf{z}_h = \mathbf{z}_h$, which would not be the case if we had used $\mathbf{I}_h$. Owing to the following fundamental result the application of $\widetilde{\mathbf{I}}_h$ to (5.20) is justified and will not affect stability.

Lemma 5.4 (Lemma 4.6 in [14]) *If* $\mathbf{u} \in \boldsymbol{H}^1(\Omega)$ *satisfies* $\mathbf{curl}\,\mathbf{u} \in \mathbf{curl}\,\widetilde{\mathbf{E}}_h$, *then*

$$\|h^{-1}(\mathbf{u}-\widetilde{\mathbf{I}}_h\mathbf{u})\|_{L^2(\Omega)} \lesssim |\mathbf{u}|_{H^1(\Omega)}\,.$$

From this lemma and (5.19) we conclude the estimate

$$\begin{aligned}\|h^{-1}\widetilde{\mathbf{I}}_h(\mathbf{z}-\mathbf{z}_h)\|_{L^2(\Omega)} &\le \|h^{-1}(\mathbf{z}-\widetilde{\mathbf{I}}_h\mathbf{z})\|_{L^2(\Omega)} + \|h^{-1}(\mathbf{z}-\mathbf{z}_h)\|_{L^2(\Omega)}\\ &\lesssim |\mathbf{z}|_{H^1(\Omega)} \lesssim \|\mathbf{curl}\,\mathbf{v}_h\|_{L^2(\Omega)}\,.\end{aligned} \tag{5.22}$$

As in Sect. 5.1, we shall now decompose $\mathbf{z}_h$ into the sum of a boundary part $\mathbf{z}_h^\partial \in \mathbf{S}_h$ and an interior part $\mathbf{z}_h^i \in \mathbf{S}_h$, where the former is defined by, *cf.* (5.8),

$$\mathbf{z}_h^\partial(\mathbf{p}) := \begin{cases}\mathbf{z}_h(\mathbf{p}) & \text{if } \mathbf{p} \in \mathcal{V}_h \cap \bar{B},\\ 0 & \text{if } \mathbf{p} \in \mathcal{V}_h \cap \Omega_0,\end{cases} \tag{5.23}$$

and the latter is supported in $\bar{\Omega}_0$:

$$\mathbf{z}_h^i := \mathbf{z}_h - \mathbf{z}_h^\partial \in \boldsymbol{H}_0^1(\Omega_0). \tag{5.24}$$

We can simply apply Lemma 5.3 to the components of $\mathbf{z}_h^\partial$ and learn

$$\left\| h^{-1}\mathbf{z}_h^\partial \right\|_{L^2(\Omega)} \lesssim \left| \mathbf{z}_h^\partial \right|_{H^1(\Omega)}, \quad \left| \mathbf{z}_h^\partial \right|_{H^1(\Omega)} \lesssim |\mathbf{z}_h|_{H^1(\Omega)}. \tag{5.25}$$

Summing up, local decompositions of $\widetilde{\mathbf{I}}_h(\mathbf{z} - \mathbf{z}_h)$ and $\mathbf{z}_h^\partial$ will be uniformly stable, but the auxiliary space has to take care of $\mathbf{z}_h^i$.

Following the policy of Sect. 5.1, we make use of another vectorial Scott-Zhang type quasi-interpolation operator $\mathbf{Q}_a : \boldsymbol{H}_0^1(\Omega_a) \mapsto \mathbf{S}_a := (S_a)^3$, that is, the vectorial version of Q_a. Then $\mathbf{w}_a := \mathbf{Q}_a\mathbf{z}_h^i \in \mathbf{S}_a \subset \widetilde{\mathbf{E}}_a$ will give the desired contribution of the auxiliary space. First note that by (5.10), (5.25), and (5.19)

$$\|\mathbf{w}_a\|_A \lesssim |\mathbf{w}_a|_{H^1(\Omega)} \lesssim \left| \mathbf{z}_h^i \right|_{H^1(\Omega)} \lesssim |\mathbf{z}_h|_{H^1(\Omega)} \lesssim \|\mathbf{curl}\, \mathbf{v}_h\|_{L^2(\Omega)}. \tag{5.26}$$

In addition, $\mathbf{w}_a$ really contains all "smooth components" of $\mathbf{z}_h^i$:

Lemma 5.5 *We have*

$$\left\| h^{-1}(\mathbf{z}_h^i - \mathbf{I}_h\mathbf{w}_a) \right\|_{L^2(\Omega)} \lesssim \left| \mathbf{z}_h^i \right|_{H^1(\Omega)}.$$

Proof We depart from the splitting

$$\mathbf{z}_h^i - \mathbf{I}_h\mathbf{w}_a = (\mathbf{z}_h^i - \mathbf{Q}_a\mathbf{z}_h^i) + (\mathbf{w}_a - \mathbf{I}_h\mathbf{w}_a). \tag{5.27}$$

First, we estimate the second term. Pick a tetrahdedron $K \in \mathcal{T}_h$ and write B for the matrix associated with the affine transformation mapping the reference ("unit") tetrahedron $\widehat{K}$ onto K. Label pulled back functions by $\widehat{\ }$ and take into account that edge element interpolation and the pullback (3.4) commute:

$$\begin{aligned}
\|\mathbf{w}_a - \mathbf{I}_h\mathbf{w}_a\|^2_{L^2(K)} &\lesssim h_K^3 \, \|\mathbf{w}_a - \mathbf{I}_h\mathbf{w}_a\|^2_{L^\infty(K)} = h_K^3 \|\mathsf{B}^{-T}(\widehat{\mathbf{w}}_a - \widehat{\mathbf{I}}_h\widehat{\mathbf{w}}_a)\|^2_{L^\infty(\widehat{K})} \\
&\lesssim h_K^3 |\mathsf{B}^{-T}|^2 \inf_{\mathbf{c}\in\mathbb{R}^3} \|(Id - \widehat{\mathbf{I}}_h)(\widehat{\mathbf{w}}_a - \mathbf{c})\|^2_{L^\infty(\widehat{K})} \lesssim h_K \, |\widehat{\mathbf{w}}_a|^2_{W^{1,\infty}(\widehat{K})} \\
&\lesssim h_K \|\mathsf{B}^T(\mathbf{grad}\mathbf{w}_a)\mathsf{B}\|^2_{L^\infty(K)} \lesssim h_K |\mathsf{B}|^4 \, |\mathbf{w}_a|^2_{W^{1,\infty}(K)}.
\end{aligned}$$

The final steps rely on the Bramble-Hilbert lemma and the obvious continuity of $\widehat{\mathbf{I}}_h$ on $W^{1,\infty}(\widehat{K})$. Using the neighborhood U_K introduced in the proof of Lemma 5.2, the local relationship

$$|\mathbf{w}_a|_{W^{1,\infty}(K_a)} = h_{K_a}^{-\frac{3}{2}} |\mathbf{w}_a|_{H^1(K_a)} \quad \forall K_a \in \mathcal{T}_a,$$

makes it possible to proceed

$$\|\mathbf{w}_a - \mathbf{I}_h\mathbf{w}_a\|^2_{L^2(K)} \lesssim h_K^5 \, |\mathbf{w}_a|^2_{W^{1,\infty}(U_K)} \lesssim h_K^2 \, |\mathbf{w}_a|^2_{H^1(U_K)}.$$

We owe this last estimate to the matching condition (4.2). Thus, the finite overlap property of the neighborhoods U_K leads to

$$\left\| h^{-1}(Id - \mathbf{I}_h)\mathbf{w}_a \right\|_{L^2(\Omega)} \lesssim |\mathbf{w}_a|_{H^1(\Omega)} ,$$

and an application of the triangle inequality together with interpolation error estimates for $\mathbf{Q}_a$ finishes the proof. □

Summing up, for $\mathbf{v}_h \in \mathbf{E}_h$ we have constructed the following decomposition

$$\mathbf{v}_h = \widetilde{\mathbf{q}}_h + \mathbf{I}_h \mathbf{w}_a + \mathbf{grad}\widetilde{\Pi}_h \phi, \tag{5.28}$$

where $\widetilde{\mathbf{q}}_h \in \widetilde{\mathbf{E}}_h$ is given by

$$\widetilde{\mathbf{q}}_h = \mathbf{z}_h^{\vartheta} + \widetilde{\mathbf{I}}_h(\mathbf{z} - \mathbf{z}_h) + (\mathbf{z}_h^i - \mathbf{I}_h \mathbf{w}_a),$$

and, by (5.22), (5.25), and Lemma 5.5, it satisfies

$$\left\| h^{-1}\widetilde{\mathbf{q}}_h \right\|_{L^2(\Omega)} \lesssim \|\mathbf{curl}\, \mathbf{v}_h\|_{L^2(\Omega)} . \tag{5.29}$$

Still, $\widetilde{\mathbf{q}}_h$ does not belong to $\mathbf{E}_h$ as required by the decomposition (4.6). Yet, by virtue of (3.12) and (3.13), we can shed the surplus:

$$\widetilde{\mathbf{q}}_h = \mathbf{q}_h + \mathbf{grad}\widetilde{\eta}_h, \quad \mathbf{q}_h \in \mathbf{E}_h,\ \eta_h \in \widetilde{S}_h, \quad \left\| h^{-1}\mathbf{q}_h \right\|_{L^2(\Omega)} \lesssim \left\| h^{-1}\widetilde{\mathbf{q}}_h \right\|_{L^2(\Omega)} .$$

This yields a modified decomposition

$$\mathbf{v}_h = \mathbf{q}_h + \mathbf{I}_h \mathbf{w}_a + \mathbf{grad}\widetilde{\theta}_h, \quad \widetilde{\theta}_h := \widetilde{\Pi}_h \phi + \widetilde{\eta}_h \in \widetilde{S}_h . \tag{5.30}$$

On the one hand, we note that (5.29) carries over to $\mathbf{q}_h$, which, therefore, meets the specification (5.17). The same is true of $\mathbf{w}_a$. On the other hand $\widetilde{\theta}_h \in \widetilde{S}_h$ seems to be a misfit. However, from (5.30) it is clear that $\mathbf{grad}\widetilde{\theta}_h \in \mathbf{E}_h$. Since the splitting (3.12) is direct, this enforces $\widetilde{\theta}_h \in S_h$! So, from now on, we will write θ_h instead of $\widetilde{\theta}_h$.

Now we can fully exploit the results of Sect. 5.1: they supply a decomposition

$$\theta_h = \zeta_h + \Pi_h \mu_a, \quad \zeta_h \in S_h,\ \mu_a \in S_a, \tag{5.31}$$

whose terms satisfy

$$\left\| h^{-1}\zeta_h \right\|_{L^2(\Omega)} \lesssim |\theta_h|_{H^1(\Omega)} , \quad |\mu_a|_{H^1(\Omega)} \lesssim |\theta_h|_{H^1(\Omega)} . \tag{5.32}$$

Merge this with (5.30) by altering $\mathbf{w}_a \leftarrow \mathbf{w}_a + \mathbf{grad}\,\mu_a \in \widetilde{\mathbf{E}}_a$. Recalling the commuting diagram property (3.7) and

$$|\theta_h|_{H^1(\Omega)} \lesssim \|\mathbf{v}_h\|_{L^2(\Omega)} + \|\mathbf{I}_h \mathbf{w}_a\|_{L^2(\Omega)} + \|\mathbf{q}_h\|_{L^2(\Omega)} \lesssim \|\mathbf{v}_h\|_A , \tag{5.33}$$

it is straightforward that we have finally obtained a decomposition (5.16) with the desired properties (5.17). As explained above, this is what it takes to prove Thm. 5.1.

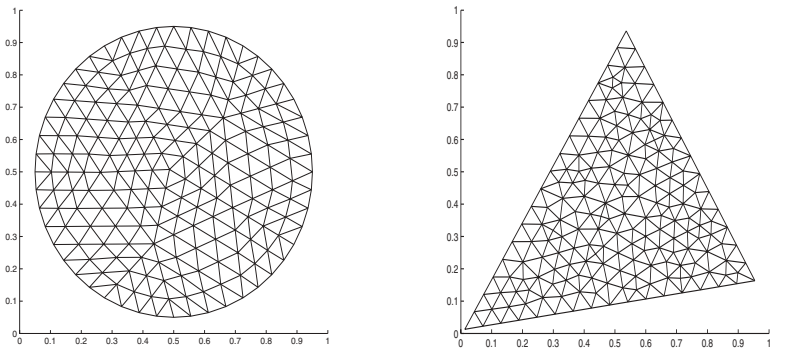

(a) Coarse circular mesh $\mathcal{C}_1$ (b) Coarse triangular mesh $\mathcal{T}_1$

Fig. 6.1 The coarsest meshes $\mathcal{C}_1$ and $\mathcal{T}_1$ used in the numerical experiments

Remark We could replace $a(\cdot,\cdot)$ by

$$a(\mathbf{u},\mathbf{v}) := \int_\Omega \mathbf{curl}\,\mathbf{u}\cdot\mathbf{curl}\,\mathbf{v}\,\mathrm{d}\mathbf{x} + \tau\int_\Omega \mathbf{u}\cdot\mathbf{v}\,\mathrm{d}\mathbf{x}\,, \quad \tau > 0. \tag{5.34}$$

A careful inspection of the proofs yields that for $\tau \ll 1$ the stabilty estimates will hold uniformly in τ. However, the constants will blow up for $\tau \to \infty$. This is also a shortcoming of analyses of multigrid in $\boldsymbol{H}(\mathbf{curl};\Omega)$ based on stable decompositions [15]. This pessimistic theoretical result is in stark contrast to the ample numerical evidence that the semi-multiplicative version of the preconditioners does not suffer when $\tau \to \infty$, see Sect. 6.

6 Numerical experiments

We first report the performance of the semi-multiplicative auxiliary space preconditioner from Sect. 4 for two two-dimensional model problems. We have decided to perform numerical studies in 2D, because in three dimensions soaring computational costs rule out the use of very fine meshes, on which the true asymptotic behavior might finally emerge. We stress that the 2D case using $\mathbf{curl}\,\mathbf{u} := \frac{\partial u_1}{\partial x_2} - \frac{\partial u_2}{\partial x_1}$ fully captures all essential features of the three-dimensional problem.

All numerical experiments rely on the bilinear form (5.34) on the domains shown in 1(a) and 1(b) equipped with a sequence of fairly uniform unstructured triangular meshes $\mathcal{C}_1,\ldots,\mathcal{C}_6$ ($\mathcal{T}_1,\ldots,\mathcal{T}_6$, respectively) that arise from successive regular refinement (plus boundary adaptation) of the coarsest meshes. The auxiliary meshes possess a regular structure and are fully covered by the unstructured meshes, see Fig. 2(a) and 2(b). In all experiments, one symmetric Gauss-Seidel sweep is chosen for hybrid smoothing and a direct solver of the problem is used in the auxiliary space.

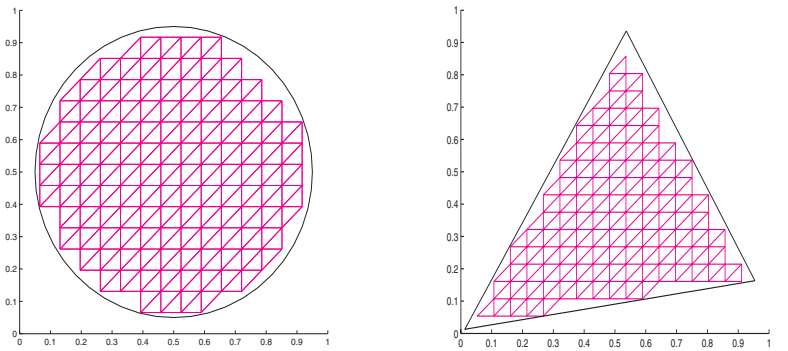

(a) Auxiliary mesh on $\mathcal{C}_1$ (b) Auxiliary mesh on $\mathcal{T}_1$

Fig. 6.2 The auxiliary meshes belonging to the coarsest triangulations

Table 6.1 Experiment 1: spectral condition numbers of $M_h^m A_h$

τ	10^{-6}	10^{-3}	1	10^3	10^6
$\mathcal{C}_1$	10.1	10.1	9.96	3.53	3.03
$\mathcal{C}_2$	9.71	9.71	9.67	5.49	3.05
$\mathcal{C}_3$	13.6	13.6	13.57	9.89	3.22
$\mathcal{C}_4$	14.3	14.3	14.3	12.5	3.38
$\mathcal{C}_5$	14.6	14.6	14.63	13.9	3.52
$\mathcal{C}_6$	12.9	12.9	12.9	12.5	5.00
$\mathcal{T}_1$	9.86	9.86	9.74	3.75	2.84
$\mathcal{T}_2$	9.10	9.10	9.07	5.16	2.89
$\mathcal{T}_3$	14.1	14.1	14.1	9.41	3.16
$\mathcal{T}_4$	13.9	13.9	13.9	11.6	3.21
$\mathcal{T}_5$	14.2	14.2	14.2	13.3	3.53
$\mathcal{T}_6$	12.2	12.2	12.1	12.0	5.25

In the experiments we monitor the spectral condition numbers of $M_h^m A_h$ and the speed of convergence of preconditioned CG iterations. Largest and smallest eigenvalues were determined by means of direct and inverse power iterations [3].

The **first experiment** examines the algorithm given in Fig. 4.3. It reports the condition number on meshes $\mathcal{C}_1/\mathcal{T}_1$ through $\mathcal{C}_6/\mathcal{T}_6$ for different values of τ in (5.34), see Tab. 6.1 for results. The condition numbers show a slight increase when the mesh is refined which is assumed to be a preasymptotic behavior, as we know that the same observation is made in the case of BPX-type preconditioners for discrete second order elliptic problems, *cf.* Rem. 2 in [3, Sect. 5]. The estimates seem to be independent of τ, which was not predicted by the theory. The mildly erratic behavior of the condition numbers is not surprising, because the local geometric relationship of the unstructured meshes and their auxiliary meshes varies on different levels of refinement.

[3] The termination criterium was a relative change of the eigenvalue estimate below 10^{-6}. Cross-checking with the MATLAB `eigs()`-routine [11, Sect. 16.5] confirmed the accuracy of the computed eigenvalues.

Table 6.2 Experiment 2: spectral condition numbers of $M_h^m A_h$

τ	10^{-6}	10^{-3}	1	10^3	10^6
$\mathcal{C}_1$	7.86	7.86	7.78	2.85	2.61
$\mathcal{C}_2$	7.41	7.41	7.38	4.34	2.68
$\mathcal{C}_3$	10.2	10.2	10.15	7.44	2.79
$\mathcal{C}_4$	10.57	10.1	10.56	9.22	2.63
$\mathcal{C}_5$	10.7	10.7	10.7	10.2	2.72
$\mathcal{C}_6$	9.00	9.00	9.00	8.74	3.61
$\mathcal{T}_1$	7.86	7.86	7.77	3.11	2.62
$\mathcal{T}_2$	7.12	7.12	7.10	4.13	2.63
$\mathcal{T}_3$	10.8	10.8	10.7	7.19	2.74
$\mathcal{T}_4$	10.3	10.3	10.3	8.64	2.59
$\mathcal{T}_5$	10.6	10.6	10.6	9.96	2.78
$\mathcal{T}_6$	8.61	8.64	8.64	8.53	3.79

The **second experiment** agrees with the first except for the use of the first family of lowest order edge elements on the auxiliary mesh. We point out that this arrangement is not covered by the theory of Sect. 5. Nevertheless, the overall behavior of the condition numbers recorded in Table. 6.2 matches that observed in the first experiment. Apparently, building V_a from second family edge elements is not essential.

In the **third experiment** we examine the performance of the semi-multiplicative auxiliary space method as a preconditioner for a preconditioned conjugate gradient iterative solver. We track the decrease of the relative error in the energy norm $||e_i||_A$ during the iteration process for the right hand side function $\mathbf{f} = (1,\ 1)^T$ in (1.1) (with $\tau = 1$ in (5.34)). The relative error $||e_i||_A$ is defined as $||e_i||_A := \frac{||\mathbf{u}_i - \mathbf{u}||_A}{||\mathbf{u}||_A}$, where $\mathbf{u}$ is the exact solution of the discretized problem and $\mathbf{u}_i$ the solution after i iterations with $\mathbf{u}_0 = 0$. Fig. 6.3 to 6.6 show the convergence of the preconditioned CG-scheme. The corresponding convergence rates are given in Tab. 6.3 and 6.4. The preconditioned CG-method displays excellent mesh-independent convergence.

In the **fourth experiment**, the semi-multiplicative scheme is replaced by the multiplicative method described in Figure 4.4. Condition numbers for all meshes in the case $\tau = 1$ are shown in Table 6.5. The condition numbers are uniformly small on all meshes, and significantly smaller than for the semi-multiplicative version of the preconditioner (at the same computational cost!).

7 Conclusion

We proposed and analyzed an auxiliary space preconditioner for $\boldsymbol{H}_0(\mathbf{curl};\Omega)$-elliptic boundary value problems discretized by means of lowest order edge elements. Theory confirms asymptotic quasi-optimality and numerical experiments demonstrate the viability of the approach. It goes without saying that the results can easily be extended to the h-version of edge elements of arbitrary but fixed polynomial degree.

So far, our investigations have focused on the case of constant coefficients. Evidently, mildly varying coefficients can be absorbed into the constants. Yet, if $a(\cdot,\cdot)$ from (1.2) featured strongly varying or anisotropic coefficients in both terms

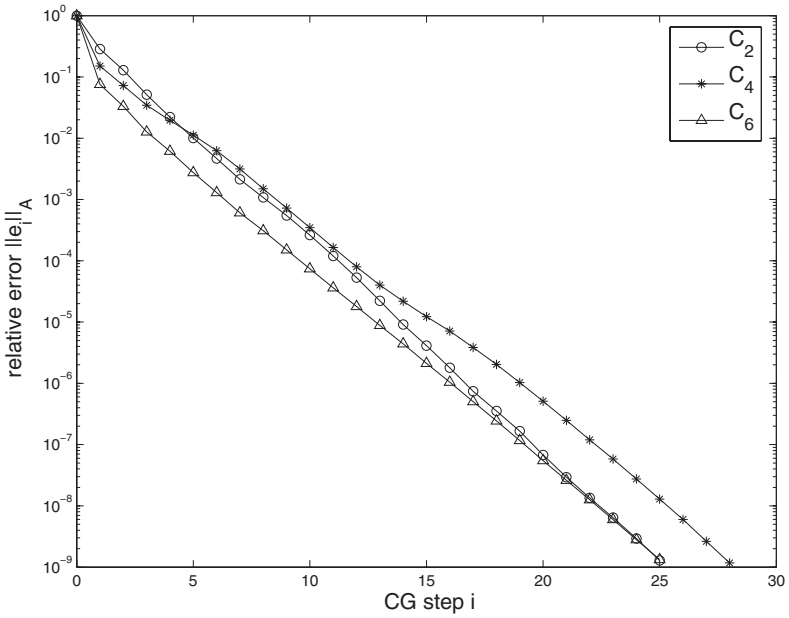

Fig. 6.3 Convergence of the preconditioned CG-method on the meshes $\mathcal{C}_2$, $\mathcal{C}_4$, $\mathcal{C}_6$ with first family of lowest order edge elements on the auxiliary mesh

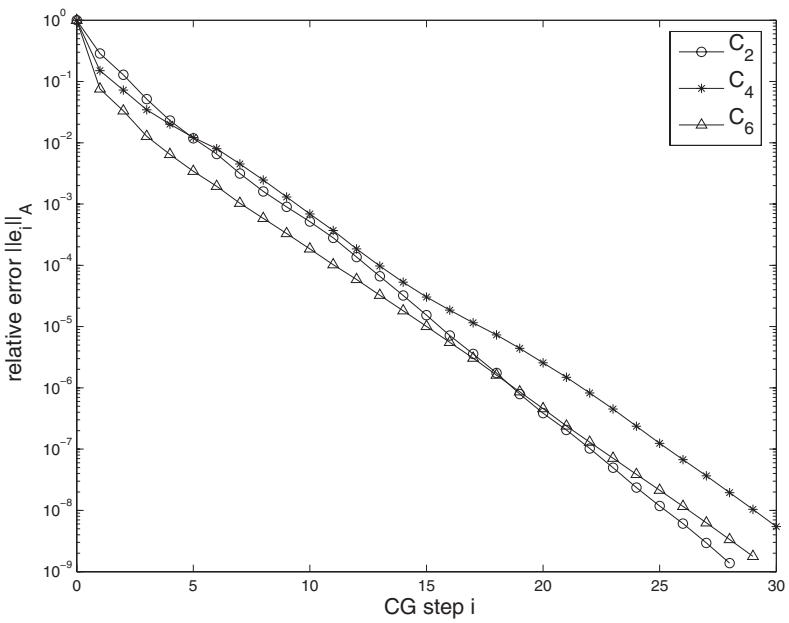

Fig. 6.4 Convergence of the preconditioned CG-method on the meshes $\mathcal{T}_2$, $\mathcal{T}_4$, $\mathcal{T}_6$ with first family of lowest order edge elements on the auxiliary mesh

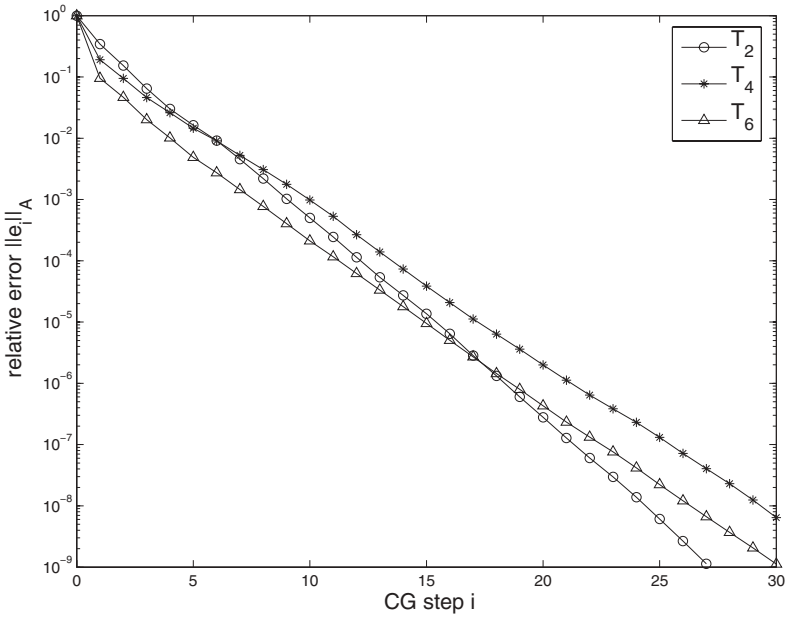

Fig. 6.5 Convergence of the preconditioned CG-scheme on the circular domain with second family of lowest order edge elements on the auxiliary mesh

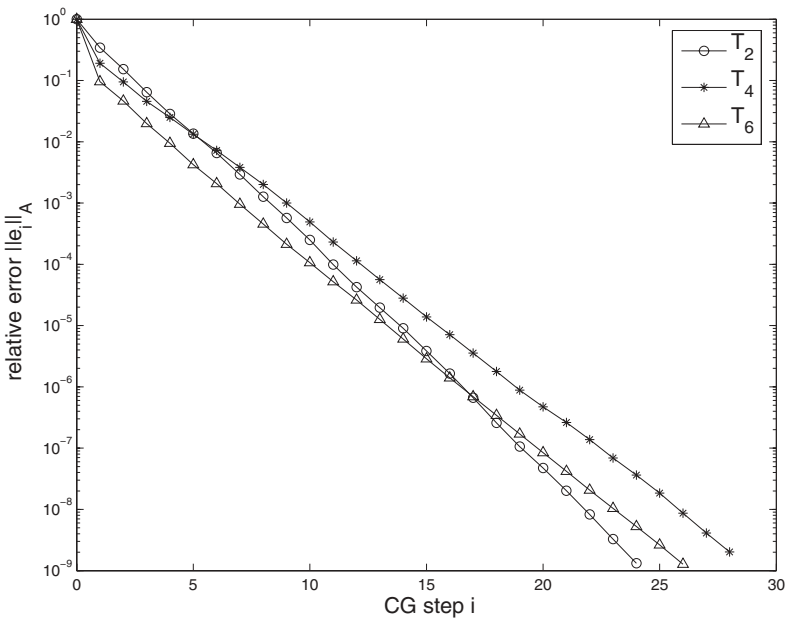

Fig. 6.6 Convergence of the preconditioned CG-scheme on the triangular domain with second family of lowest order edge elements on the auxiliary mesh

Table 6.3 Experiment 3: preconditioned CG convergence rates (second family of lowest order edge elements on auxiliary mesh)

	$\mathcal{C}_1$	$\mathcal{C}_2$	$\mathcal{C}_3$	$\mathcal{C}_4$	$\mathcal{C}_5$	$\mathcal{C}_6$
$\sqrt[5]{\frac{\|e_6\|_A}{\|e_1\|_A}}$	0.1696	0.4118	0.2046	0.4144	0.1367	0.3214
$\sqrt[5]{\frac{\|e_{11}\|_A}{\|e_6\|_A}}$	0.2312	0.5345	0.2934	0.5629	0.3483	0.5578
$\sqrt[5]{\frac{\|e_{16}\|_A}{\|e_{11}\|_A}}$	0.2420	0.4951	0.3261	0.5351	0.3049	0.5586
$\sqrt[5]{\frac{\|e_{21}\|_A}{\|e_{16}\|_A}}$	0.2795	0.4788	0.3347	0.6102	0.3646	0.5390
$\sqrt[5]{\frac{\|e_{26}\|_A}{\|e_{21}\|_A}}$	0.2063	0.4979	0.2883	0.5461	0.2817	0.5417
	$\mathcal{T}_1$	$\mathcal{T}_2$	$\mathcal{T}_3$	$\mathcal{T}_4$	$\mathcal{T}_5$	$\mathcal{T}_6$
$\sqrt[5]{\frac{\|e_6\|_A}{\|e_1\|_A}}$	0.2337	0.4389	0.2106	0.4290	0.1365	0.3447
$\sqrt[5]{\frac{\|e_{11}\|_A}{\|e_6\|_A}}$	0.2592	0.4984	0.3543	0.5833	0.3212	0.5339
$\sqrt[5]{\frac{\|e_{16}\|_A}{\|e_{11}\|_A}}$	0.2061	0.4866	0.2799	0.5234	0.3441	0.5376
$\sqrt[5]{\frac{\|e_{21}\|_A}{\|e_{16}\|_A}}$	0.2334	0.4593	0.3074	0.5532	0.3385	0.5385
$\sqrt[5]{\frac{\|e_{26}\|_A}{\|e_{21}\|_A}}$	0.2068	0.4651	0.2703	0.5802	0.2717	0.5534

Table 6.4 Experiment 3: preconditioned CG convergence rates (first family of lowest order edge elements on auxiliary mesh)

	$\mathcal{C}_1$	$\mathcal{C}_2$	$\mathcal{C}_3$	$\mathcal{C}_4$	$\mathcal{C}_5$	$\mathcal{C}_6$
$\sqrt[5]{\frac{\|e_6\|_A}{\|e_1\|_A}}$	0.1611	0.3989	0.1989	0.4074	0.1308	0.3075
$\sqrt[5]{\frac{\|e_{11}\|_A}{\|e_6\|_A}}$	0.1746	0.4817	0.2369	0.4988	0.2607	0.4851
$\sqrt[5]{\frac{\|e_{16}\|_A}{\|e_{11}\|_A}}$	0.2124	0.4358	0.2694	0.5123	0.2759	0.4915
$\sqrt[5]{\frac{\|e_{21}\|_A}{\|e_{16}\|_A}}$	0.2357	0.4397	0.2818	0.5298	0.2700	0.4812
$\sqrt[5]{\frac{\|e_{26}\|_A}{\|e_{21}\|_A}}$	0.1371	0.4523	0.1871	0.4794	0.2166	0.4756
	$\mathcal{T}_1$	$\mathcal{T}_2$	$\mathcal{T}_3$	$\mathcal{T}_4$	$\mathcal{T}_5$	$\mathcal{T}_6$
$\sqrt[5]{\frac{\|e_6\|_A}{\|e_1\|_A}}$	0.2255	0.4233	0.2042	0.4214	0.1291	0.3353
$\sqrt[5]{\frac{\|e_{11}\|_A}{\|e_6\|_A}}$	0.2079	0.4495	0.2782	0.5170	0.2527	0.4787
$\sqrt[5]{\frac{\|e_{16}\|_A}{\|e_{11}\|_A}}$	0.1695	0.4342	0.2321	0.4899	0.3089	0.4850
$\sqrt[5]{\frac{\|e_{21}\|_A}{\|e_{16}\|_A}}$	0.2040	0.4150	0.2609	0.5085	0.2520	0.4942
$\sqrt[5]{\frac{\|e_{26}\|_A}{\|e_{21}\|_A}}$	0.1523	0.4081	0.2129	0.5234	0.2277	0.5000

we have to resign to a gross deterioration of the constants in the theoretical estimates. As far as implementation is concerned, if the coefficients for the second and zero order term of $a(\cdot,\cdot)$ display completely different behavior it might be advisable to use different bilinear forms on the auxiliary space for the treatment of gradient components and **curl**-carrying components. The efficacy of this idea remains to be investigated.

Table 6.5 Experiment 4: spectral condition numbers (first and second family of lowest order edge elements on auxiliary mesh)

	$\mathcal{C}_1$	$\mathcal{C}_2$	$\mathcal{C}_3$	$\mathcal{C}_4$	$\mathcal{C}_5$	$\mathcal{C}_6$
first family	3.72	3.83	4.50	4.36	4.24	3.75
second family	3.83	3.84	4.71	4.65	4.62	4.32
	$\mathcal{T}_1$	$\mathcal{T}_2$	$\mathcal{T}_3$	$\mathcal{T}_4$	$\mathcal{T}_5$	$\mathcal{T}_6$
first family	4.33	3.84	5.58	4.85	5.15	3.97
second family	4.33	3.94	5.74	5.19	5.53	4.29

References

1. Arnold, D., Falk, R., Winther, R.: Multigrid in $H(\mathrm{div})$ and $H(\mathbf{curl})$. Numer. Math. **85**, 175–195 (2000)
2. Bochev, P., Garasi, C., Hu, J., Robinson, A., Tuminaro, R.: An improved algebraic multigrid method for solving Maxwell's equations. SIAM J. Sci. Comp. **25**, 623–642 (2003)
3. Bornemann F., A sharpedned condition number estimate for the BPX-preconditioner of elliptic finite element problems on highly non-uniform triangulations, Tech. Report SC 91-9, ZIB, Berlin, Germany, September 1991
4. Bossavit, A.: Two dual formulations of the 3D eddy–currents problem. COMPEL, **4**, 103–116 (1985)
5. Chan, T., Zou, J.: A convergence theory of multilevel additive schwarz methods on unstructured meshes. Numerical Algorithms, **13**, 365–398 (1996)
6. Chan, T.F., Smith, B.F., Zou, J.: Overlapping schwarz methods on unstructured meshes using non-matching coarse grids. Numer. Math. **73**, 149–167 (1996)
7. Girault, V., Raviart, P.: Finite element methods for Navier–Stokes equations. Springer, Berlin, 1986
8. Gopalakrishnan, J., Pasciak, J.: Overlapping schwarz preconditioners for indefinite time harmonic Maxwell equations. Math. Comp. **72**, 1–15 (2003)
9. Gopalakrishnan, J., Pasciak, J., Demkowicz, L.: Analysis of a multigrid algorithm for time harmonic Maxwell equations. SIAM J. Numer. Anal. **42**, 90–108 (2003)
10. Griebel, M., Oswald, P.: On the abstract theory of additive and multiplicative schwarz algorithms. Numer. Math. **70**, 163–180 (1995)
11. Hanselman, D., Littlefield, B.: Mastering MATLAB 6. Prentice Hall, Upper Saddle River, NJ, 2001
12. Hiptmair, R.: Multigrid method for Maxwell's equations. SIAM J. Numer. Anal. **36**, 204–225 (1999)
13. Hiptmair, R.: Discrete Hodge operators. Numer. Math. **90**, 265–289 (2001)
14. Hiptmair, R.: Finite elements in computational electromagnetism. Acta Numerica, **11**, 237–339 (2002)
15. Hiptmair, R.: Analysis of multilevel methods for eddy current problems. Math. Comp. **72**, 1281–1303 (2003)
16. Hiptmair, R., Toselli, A.: Overlapping and multilevel Schwarz methods for vector valued elliptic problems in three dimensions. In: Parallel Solution of Partial Differential Equations, Bjorstad P. and M. Luskin, eds. no. 120 in IMA Volumes in Mathematics and its Applications, Springer, Berlin, (1999), pp. 181–202.
17. Hu, Q., Zou, J.: A non-overlapping domain decomposition method for Maxwell's equation in three dimensions. SIAM J. Numer. Anal. **41**, 1682–1708 (2003)
18. Hu, Q., Zou, J.: Substructuring preconditioners for saddle-point problems arising from Maxwell's equations in three dimensions. Math. Comp. **73**, 35–61 (2003)
19. Nédélec, J.: Mixed finite elements in $\mathbb{R}^3$. Numer. Math. **35**, 315–341 (1980)
20. Nédélec, J.: A new family of mixed finite elements in R^3. Numer. Math. **50**, 57–81 (1986)
21. Pasciak, J., Zhao, J.: Overlapping Schwarz methods in H(curl) on polyhedral domains. J. Numer. Math. **10**, 221–234 (2002)
22. Reitzinger, S., Schöberl, J.: Algebraic multigrid for edge elements. Numerical Linear Algebra with Applications, **9**, 223–238 (2002)
23. Ruge, J., Stüben, K.: Algebraic multigrid. In: McCormick, S. (ed.), Multigrid methods, Frontiers in Applied Mathematics, SIAM, Philadelphia, 1987, ch. 4, pp. 73–130

24. Scott, L.R., Zhang, Z..: Finite element interpolation of nonsmooth functions satisfying boundary conditions Math. Comp. **54**, 483–493 (1990)
25. Sterz, O.: Multigrid for time-harmonic eddy currents without gauge. Preprint 2003-07, IWR Heidelberg, Heidelberg, Germany, April 2003
26. Stüben, K.: An introduction to algebraic multigrid. Academic Press, London, ch. Appendix A, 2001, pp. 413–528
27. Toselli, A.: Overlapping Schwarz methods for Maxwell's equations in three dimensions. Numer. Math. **86**, 733–752 (2000)
28. Xu, J.: Iterative methods by space decomposition and subspace correction. SIAM Review, **34**, 581–613 (1992)
29. Xu, J.: The auxiliary space method and optimal multigrid preconditioning techniques for unstructured grids. Computing, **56**, 215–235 (1996)
30. Xu, J.: An introduction to multilevel methods. In: M. Ainsworth, K. Levesley, M. Marletta, W. Light (eds.), Wavelets, Multilevel Methods and Elliptic PDEs, Numerical Mathematics and Scientific Computation, Oxford: Clarendon Press, 1997, pp. 213–301
31. Xu, J., Zou, J.: Some non-overlapping domain decomposition methods. SIAM Review, **40**, 857–914 (1998)